Electronic Supplementary Material (ESI) for CrystEngComm.

Electronic supplementary information

Hollow single-crystalline octahedra of hydrated/dehydrated hydroxyl ferric phosphate and crystal water enhanced electrochemical properties of the hydrated sample for the reversible lithiation-delithiation

*Xiaoli Ma, Hongrui Jiang, Fanghui Tian, Yamei Ti, Miaomiao Zhang, Qiang Shen**

Key Laboratory for Colloid and Interface Chemistry of Education Ministry, School of Chemistry and Chemical Engineering, Shandong University, Jinan 250100, China (E-mail: qshen@sdu.edu.cn*).*

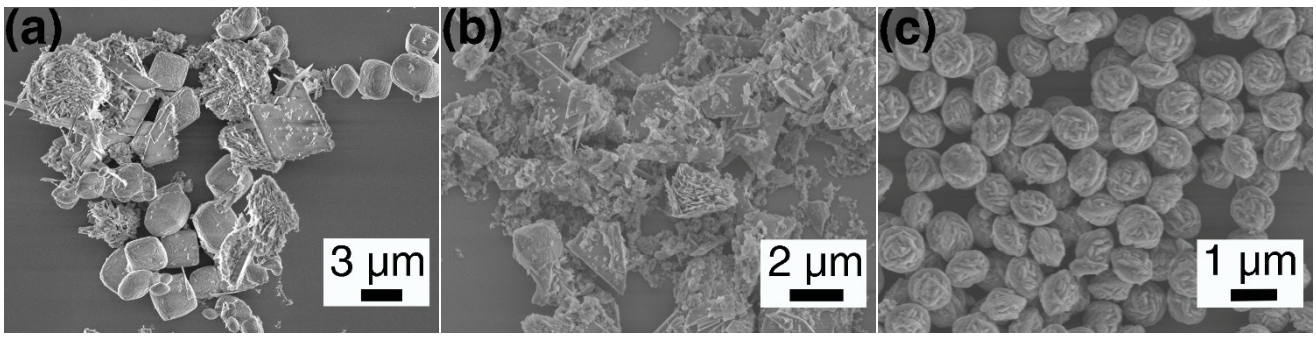

Fig. S1 SEM images of precipitates obtained using the non-(1,2-propanediol) solvents of (a) n-propanol, (b) isopropanol and (c) ethanediol to dissolve solid-state $FeCl_3$, respectively.

As for the 48-h solution-based reaction of $FeCl_3$ with H_3PO_4 at 140°C, there is absolutely no precipitates when 1,2,3-propanetriol is substituted for 1,2-propanediol.

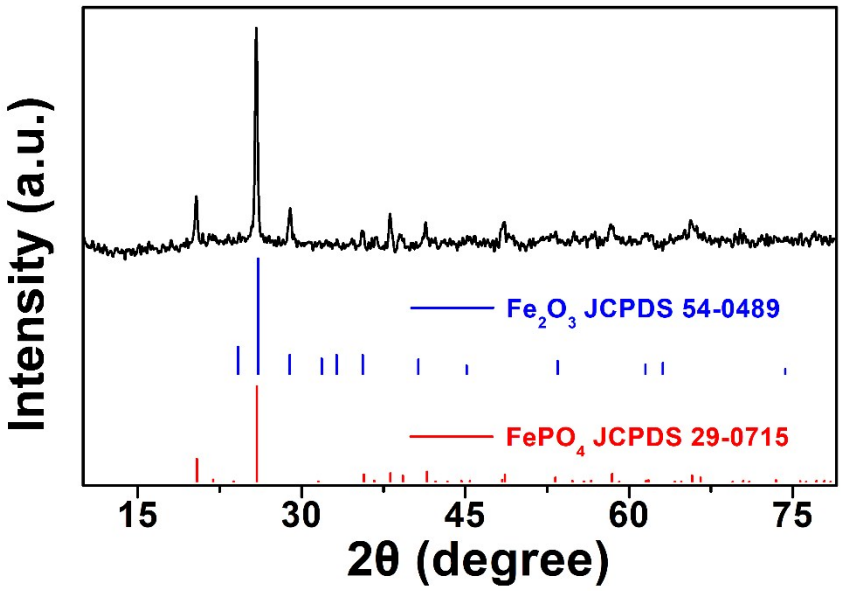

Fig. S2 XRD pattern of the air-atmosphere heat-treated products of $Fe_5(PO_4)_4(OH)_3{\cdot}2H_2O$ octahedra at 700℃ for 8 h, exhibiting the co-existence of $FePO_4$ (JCPDS No. 29-0715) and Fe_2O_3 crystals (JCPDS No. 54-0489).

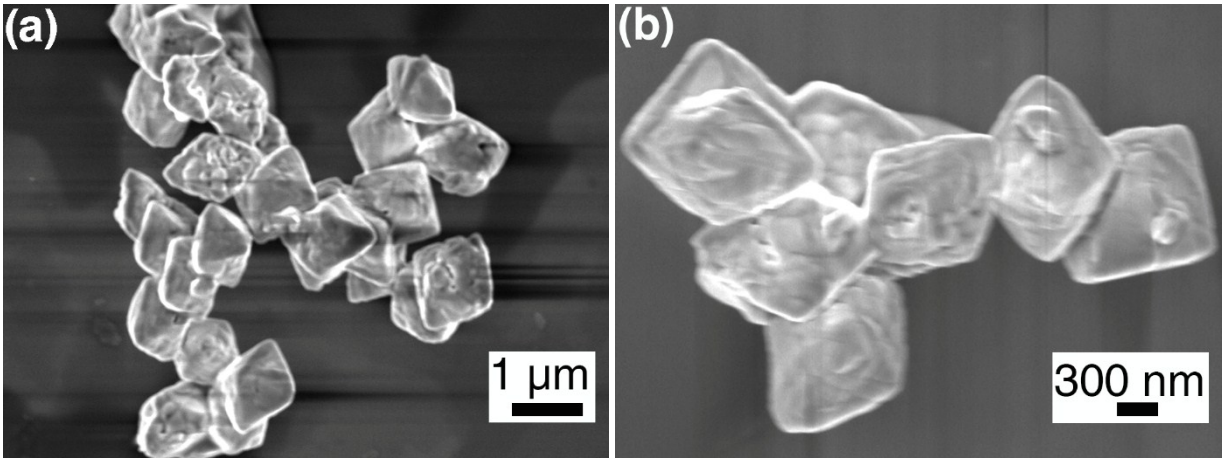

Fig. S3 SEM images of the air-atmosphere heat-treated products of $Fe_5(PO_4)_4(OH)_3{\cdot}2H_2O$ octahedra at 700℃ for 8 h.

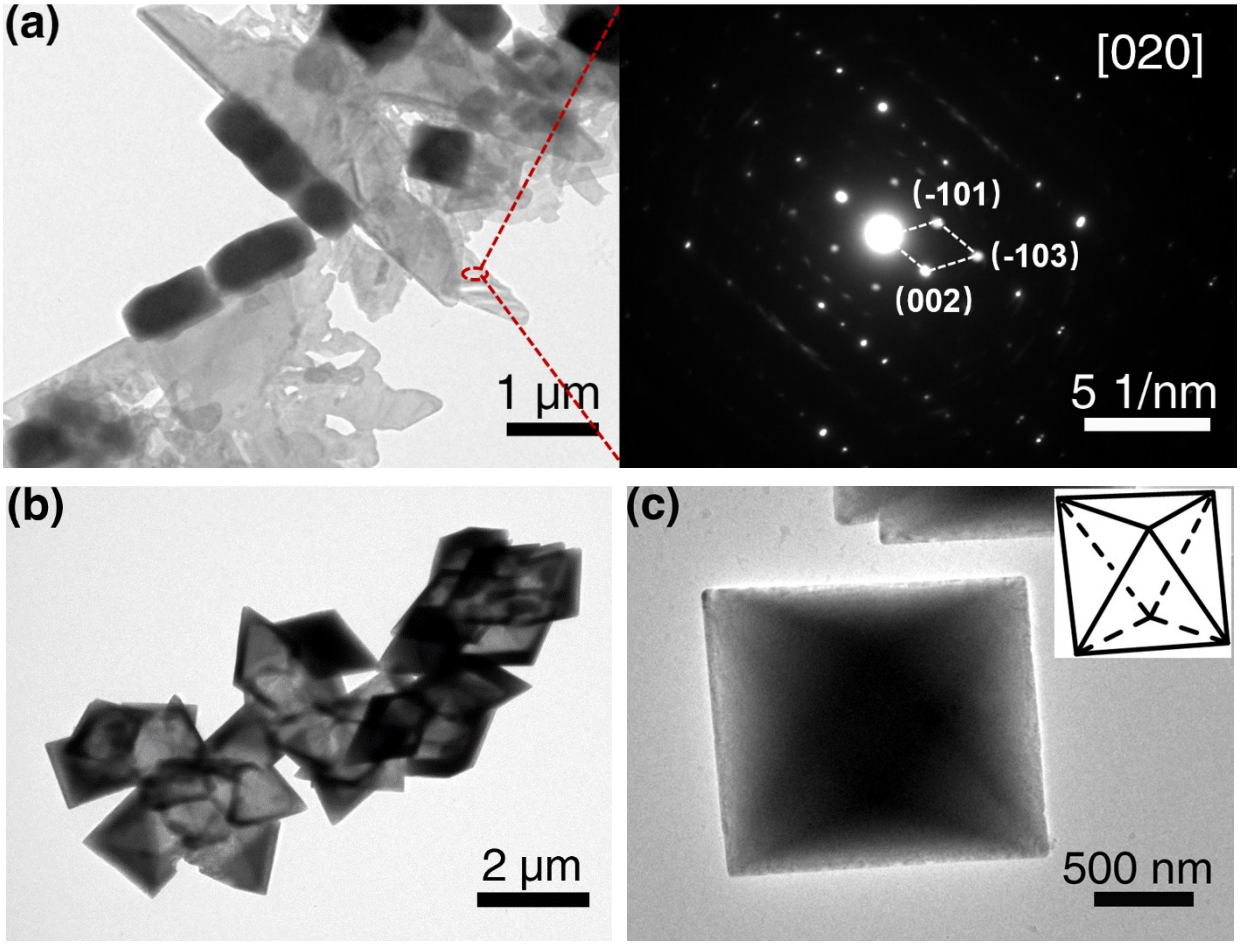

Fig. S4 TEM images of precipitates collected at an incubation time of (a) 16 and (b, c) 48 h, respectively. In panel (a), an ellipse area was marked to obtain the SAED pattern of $FePO_4 \cdot 2H_2O$ sheet-like structure, while in panel (c) the corresponding edge outlines of a regular octahedron is shown as an inset.

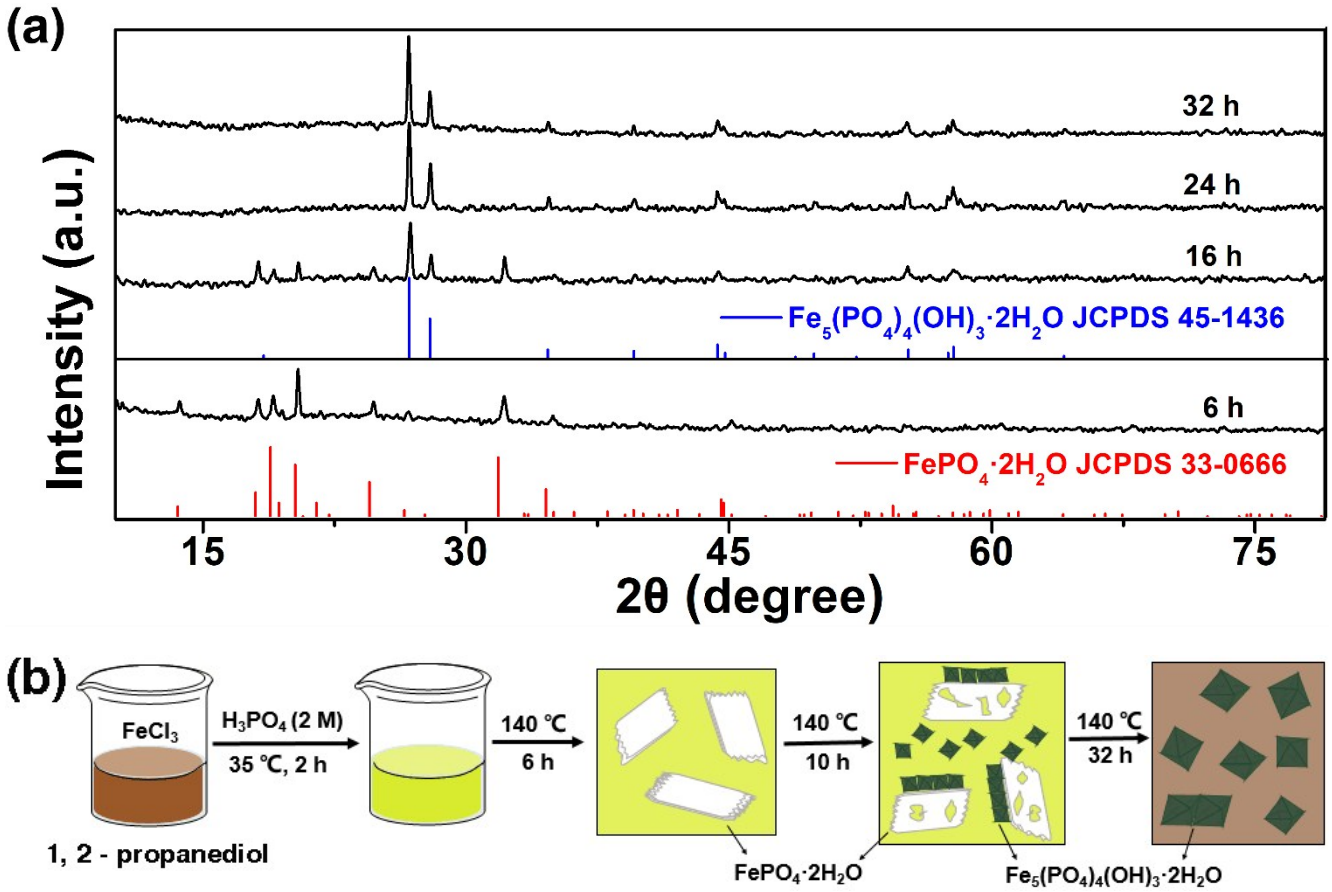

Fig. S5 (a) XRD patterns of intermediates collected at the incubation times of 6, 16, 24 and 32 h, and the standard reflection data of monoclinic $FePO_4 \cdot 2H_2O$ (JCPDS No. 33-0666) and orthorhombic $Fe_5(PO_4)_4(OH)_3 \cdot 2H_2O$ (JCPDS No. 45-1436) are also enclosed. (b) Schematic diagram for the formation process of $Fe_5(PO_4)_4(OH)_3 \cdot 2H_2O$ hollow single-crystalline octahedra, and the colors of initial solutions and subsequent supernatants and precipitates are also shown simultaneously.

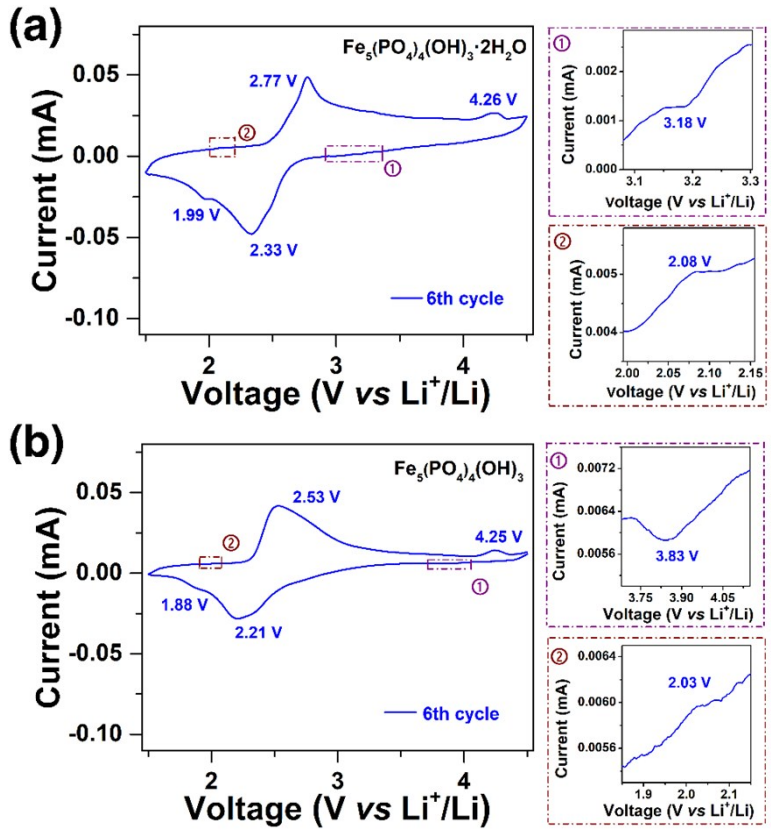

Fig. S6 The 6th-cycle CV curve of (a) $Fe_5(PO_4)_4(OH)_3·2H_2O$ and (b) $Fe_5(PO_4)_4(OH)_3$ electrodes operated at 0.1 mV s^{-1}, respectively. In each panel, the marked regions were magnified and shown alongside of the panel.

In the presence and absence of crystal water in FeO_6/PO_4 lattice structures, by magnification three pairs of CV anodic/cathodic redox peaks could be detected, respectively: 4.26/3.18, 2.77/2.33 and 2.08/1.99 V ($Fe_5(PO_4)_4(OH)_3·2H_2O$); 4.25/3.83, 2.53/2.21 and 2.03/1.88 V ($Fe_5(PO_4)_4(OH)_3$).

Certainly, the anodic/cathodic redox peaks of 2.77/2.33 and 2.53/2.21 V should be assigned to the delithiation/lithiation of the hydrated and dehydrated samples (i.e., the Fe^{2+}/Fe^{3+}-based redox reactions within $FePO_4$-comment lattices), respectively.

According to the literature results, the anodic/cathodic redox peaks of 4.26/3.18 or 4.25/3.83 V may be associated with a $Fe(OH)_3$-components' OH^--relative reversible transformation.[1-3].

Accompanied by this OH^--relative reversible electrochemical reaction, in $Fe(OH)_3$-like domains Fe^{2+}/Fe^{3+}-based redox reaction may simultaneously occur,[4] which could explain the CV anodic/cathodic redox peaks of 2.08/1.99 and 2.03/1.88 V for $Fe_5(PO_4)_4(OH)_3·2H_2O$ and $Fe_5(PO_4)_4(OH)_3$, respectively.

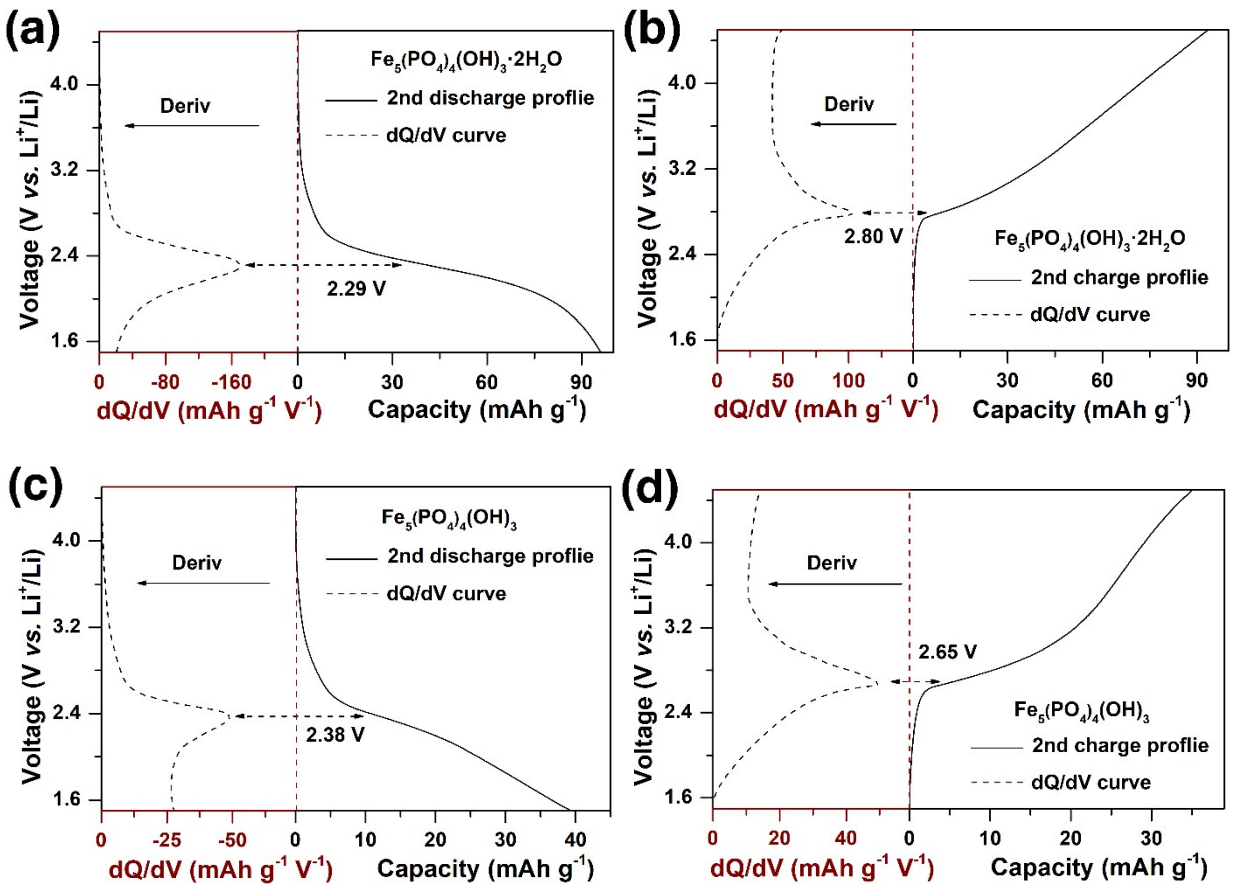

Fig. S7 The combination of the discharge/charge profiles at 50 mA g^{-1} in the 2nd cycle with the corresponding differential capacity against voltage (dQ/dV) curves of (a, b) $Fe_5(PO_4)_4(OH)_3 \cdot 2H_2O$ and (c, d) $Fe_5(PO_4)_4(OH)_3$ hollow single-crystalline octahedra, respectively.

Although there exist the ambiguous potential plateaus in these representative discharge-charge profiles of the hydrated/dehydrated samples, the "exact" potential plateaus could also be determined using the combination of the discharge/charge profiles with the corresponding dQ/dV curves.

As shown in panel (a) or (b), the cathodic or anodic plateau potential of $Fe_5(PO_4)_4(OH)_3 \cdot 2H_2O$ localizes around 2.29 or 2.80 V *vs.* Li^+/Li, and as shown in panel (c) or (d), that of $Fe_5(PO_4)_4(OH)_3$ appears around 2.38 and 2.65 V *vs.* Li^+/Li corresponding. Herein, these plateau potentials are slightly different with the corresponding CV cathodic/anodic peak positions, which could be assigned to the different operation conditions.

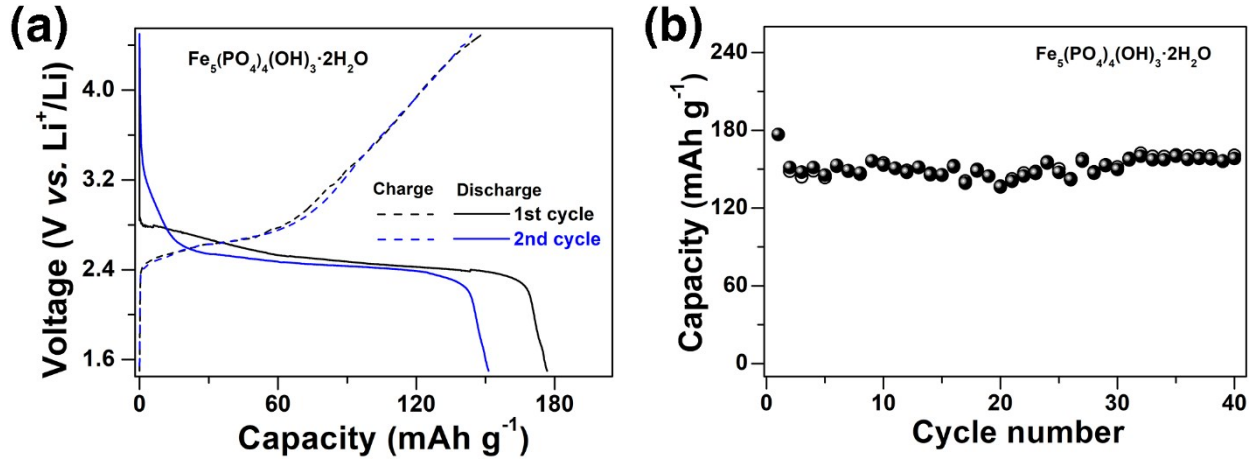

Fig. S8 (a) Voltage profiles and (b) cycling performance of $Fe_5(PO_4)_4(OH)_3 \cdot 2H_2O$ electrode operated at a low current rate of 5 mA g^{-1}, showing an extremely high initial discharge capacity of 176.7 mAh g^{-1} in panel (a) and a reversible value of 158.2 mAh g^{-1} in the 40th cycle in panel (b).

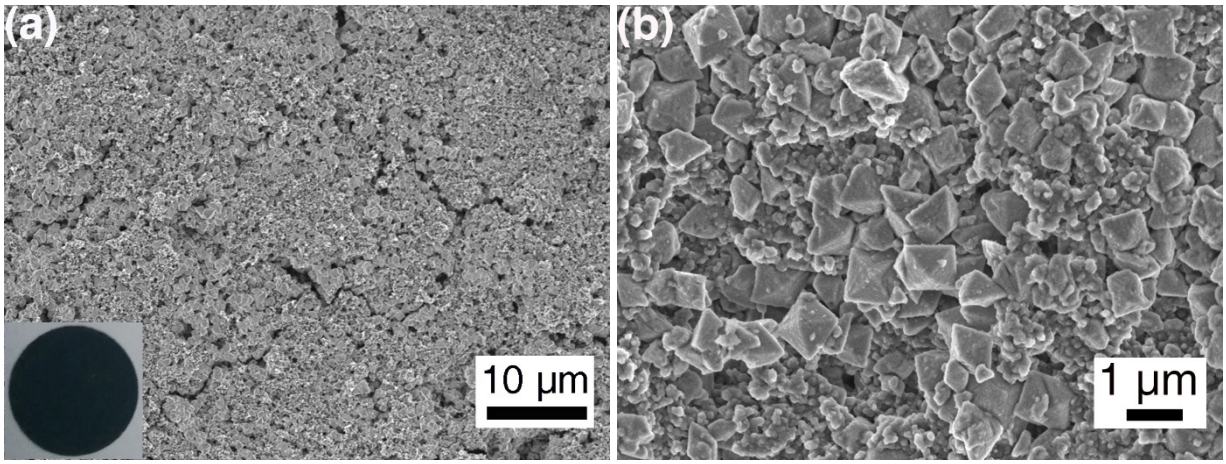

Fig. S9 (a, b) SEM images of an electrochemically cycled $Fe_5(PO_4)_4(OH)_3$ electrode after the 100th cycle at 100 mA g^{-1}, and in panel (a) optical micrograph of the electrode was shown as an inset.

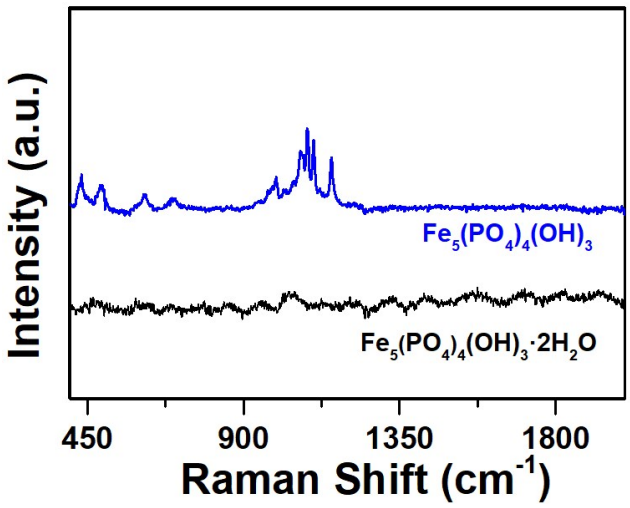

Fig. S10 Raman spectra of $Fe_5(PO_4)_4(OH)_3 \cdot 2H_2O$ and $Fe_5(PO_4)_4(OH)_3$ samples.

According to literature results,[5-9] $Fe_5(PO_4)_4(OH)_3$ Raman peaks within the wavenumber region of 900 and 1200 cm^{-1} can be attributed to the PO_4 stretching bands and the others within the region from 400 to 600 cm^{-1} can be assigned to the PO_4 bending bands.

It is very reproducible that no Raman signals of $Fe_5(PO_4)_4(OH)_3 \cdot 2H_2O$ could be detected within the full region from 400 to 2000 cm^{-1}.

References

1. N. Dupre, J. Gaubicher, T. L. Mercier, G. Wallez, J. Angenault and M. Quarton, *Solid State Ionics*, 2001, **140**, 209-221.
2. C. Delacourt, P. Poizot, D. Bonnin and C. Masquelier, *J. Electrochem. Soc.*, 2009, **156**, A595-A605.
3. X. Tan, R. Liu, C. Xie and Q. Shen, *J. Power Sources*, 2018, **374**, 134-141.
4. M. Zhang, J. *Alloy. Compd.*, 2015, **648**, 134-138.
5. S. Han, J. Wang, S. Li, D. Wu and X. Feng, *J. Mater. Chem. A*, 2014, **2**, 6174-6179.
6. S. W. Kim, J. Ryu, C. B. Park and K. Kang, *Chem. Commun.*, 2010, **46**, 7409-7411.
7. J. Qian, M. Zhou, Y. Cao, X. Ai and H. Yang, *J. Phys. Chem. C*, 2011, **114**, 3477-3482.
8. N. Marx, L. Croguennec, D. Carlier, L. Bourgeois, P. Kubiak, F. d. r. L. Cras and C. Delmas, *Chem. Mater.*, 2010, **22**, 1854-1861.
9. Y. Fang, L. Xiao, J. Qian, X. Ai, H. Yang and Y. Cao, *Nano Lett.*, 2014, **14**, 3539-3543.